An NMR Technique for the Analysis of Pore Structure: Application to Mesopores and Micropores

DAVID P. GALLEGOS,* DOUGLAS M. SMITH,* AND C. JEFFERY BRINKER†

*UNM Powders and Granular Materials Laboratory, Department of Chemical and Nuclear Engineering, University of New Mexico, Albuquerque, New Mexico 87131, and †Division 1846, Sandia National Laboratories, Albuquerque, New Mexico 87185

Received June 15, 1987; accepted August 17, 1987

The use of NMR spin-lattice relaxation experiments on water, or other proton-containing fluids, in a porous solid as a pore structure/size measurement tool has been recently reported for porous solids with pore size greater than $\approx$5 nm. This approach has numerous advantages, as compared to nitrogen sorption/condensation and mercury porosimetry, including no network/percolation effects, no pore shape assumption is required, wet materials may be analyzed, and small specific pore volumes may be studied. Assumptions used to relate the measured spin-lattice relaxation time, T_1, to the pore size limit the application of the method to pore sizes greater than 5 nm. In this work, we explore the extension of this NMR technique to porous solids with pores in the micropore and mesopore size ranges.

By comparing previously published results of the relative distribution of surface- and bulk-phase water as a function of pore size (E. Almagor and G. J. Belfort, *J. Colloid Interface Sci.* **66**, 146, (1978)) to predictions from various pore models, we have demonstrated that the "two-fraction, fast exchange" model may be applied to relate measured T_1 to pore size in the mesopore and micropore size range if the pore geometry is known (or assumed). For pore size greater than 5 nm, pore geometry is not important. Comparisons between conventional techniques, such as nitrogen sorption and mercury porosimetry, and the results of NMR spin-lattice relaxation experiments are complicated by the fact that different pore structure parameters are measured with these methods. Despite this, agreement between the methods is quite good for the five sol–gel-derived materials which we have studied.

INTRODUCTION

Recently, Gallegos, Smith, and co-workers (1, 2) have demonstrated the viability of extracting pore structure information from NMR spin-lattice relaxation measurements. This technique has several advantages as compared to conventional pore structure analysis techniques such as mercury porosimetry and nitrogen adsorption/condensation. These advantages include the ability to study wet materials (i.e., the pore structure of some materials may change significantly during drying), the determination of the "true" hydraulic radius, and the absence of network/percolation effects. In addition, this technique is fast, nondestructive, and no limitation on sample size exists. The ability to study materials with very small total pore volume such as porous thin films/membranes is of special interest.

The principle of this NMR approach is that fluid, usually water, contained in the pore space of a solid will relax at a faster rate than bulk fluid during a spin-lattice relaxation experiment (i.e., pore fluid will have a shorter spin-lattice relaxation decay time, T_1). Since a porous solid will have a range of pore sizes, a distribution of T_1 will exist which is related to the desired pore size distribution and must be extracted from the observed magnetization relaxation data. The extraction of discrete $f(T_1)$ distributions using a nonnegative least-squares approach has been described by Munn and Smith (3). Gallegos and Smith (2) and Brown and co-workers (4) used a regularization technique to successfully extract continuous $f(T_1)$ distributions.

0021-9797/88 $3.00

In order to relate the calculated $f(T_1)$ to the desired pore size distribution, previous investigators (1, 2, 4) used the "two-fraction, fast exchange" model of Brownstein and Tarr (5). The pore fluid is assumed to contain two separate phases: a surface phase which has a much smaller relaxation time and a bulk phase which has the same properties as a fluid which is not in a porous solid. If diffusion between the two phases is fast compared to the relaxation times, then the observed T_1 for the pore is given by

$$1/T_1 = f_b/T_{1b} + f_s/T_{1\ \text{surface}}, \qquad [1]$$

where f_b and f_s are the relative volume fractions of the bulk and surface phases. The thickness of this surface-affected phase, Δ, was found to be one or two monolayers for the hectorite–water system by Woessner (6) and for the glass–water system by Belfort, Schering, and Seevers (8) and Almagor and Belfort (7). However, Almagor and Belfort note a difference between the molecular correlation times of the first and second monolayer of the surface phase.

In order to use Eq. [1] for pore structure analysis, the volume fractions of the two phases, f_b and f_s, must be related to the pore size. If the surface area and total volume of a pore is SA and PV, then f_b and f_s are given by

$$f_s = \Delta SA/PV, \quad f_b = 1 - \Delta SA/PV. \qquad [2]$$

If the volume of the surface phase is taken to be much smaller than the bulk phase ($f_b \gg f_s$), Eq. [1] may be written as

$$1/T_1 = 1/T_{1b} + \Delta SA/(PVT_{1\ \text{surface}}). \qquad [3]$$

Defining the characteristic pore size as the hydraulic radius, $r_p = 2PV/SA$,

$$1/T_1 = 1/T_{1b} + 2\Delta/T_{1\ \text{surface}}/r_p. \qquad [4]$$

In practice, the surface parameters may be grouped into a surface relaxation time, T_{1s}, which is $T_{1\ \text{surface}}/\Delta$. Simplifying, the working equation for relating T_1 to pore radius used by Brown and co-workers (4) and Gallegos, Smith, and co-workers (1, 2) is

$$1/T_1 = \alpha + \beta/r_p, \qquad [5]$$

where α is $1/T_{1b}$ and is a function of the fluid, temperature, and field strength only. β is $2/T_{1s}$ and is a function of the pore fluid, temperature, field strength, and pore surface chemistry. In the derivation of Eq. [5], no assumptions concerning pore shape have been made other than defining the pore radius as the hydraulic radius. However, by assuming that the volume of the surface phase is much smaller than the volume of the bulk phase, the applicability of Eq. [5] is limited to pore sizes greater than ≈ 5 nm.

In this work, we intend to extend the validity of NMR pore structure analysis to pore sizes in the radius range of 0.5 to 5.0 nm. This mesopore/micropore size range is of considerable interest in many practical applications. In addition to extending the "two-fraction, fast exchange" model to these smaller pore sizes, we will demonstrate NMR analysis of pores in this size range for a number of xerogels. These results will be compared to nitrogen adsorption/condensation, mercury porosimetry, and gas permeation pore structure measurements.

THEORY

The lower pore radius limit of 5 nm for the application of Eq. [5] is caused by the assumption of negligible surface-phase volume as compared to the volume of the bulk phase. This limit is not caused by a failure of the "two-fraction, fast exchange" model, Eq. [1], which will be valid for smaller pore sizes as long as separate surface and bulk phases exist. Thus, the problem of extending Eq. [1] to smaller pore size is how to correctly account for the volume of the surface phase. This can only be accomplished by making an assumption concerning the pore shape. The use of an assumption concerning the pore shape does not necessarily imply a decrease in the utility of NMR pore structure analysis as compared to conventional approaches. With porosimetry and condensation, a pore assumption must be made to relate applied pressure (porosimetry) or relative pressure (condensation) to pore size.

If the pore is assumed to be formed by two

flat plates of spacing equal to $2R$ or a cylinder of radius R or a spherical cavity of radius R, Eq. [1] may be written

$$1/T_1 = [1 - \Delta/R]^n/T_{1b} + [1 - (1 - \Delta/R)^n]/T_{1\ \text{surface}}, \quad [6]$$

where

$n = 1$, flat plate
$n = 2$, cylinder
$n = 3$, spherical cavity.

For larger pores, the observed spin-relaxation time is related to the pore size by two parameters, α and β. For pores in the mesopore and micropore size regions, a third parameter related to the thickness of the surface layer is required. For a flat plate pore model and using α, β, and Δ, Eq. [6] becomes

$$1/T_1 = \alpha + \beta(\tfrac{1}{2} - \Delta\alpha/\beta)/R. \quad [7]$$

For flat plates, the hydraulic radius, r_p, is $2R$ and Eq. [7] becomes

$$1/T_1 = \alpha + \beta(1 - 2\Delta\alpha/\beta)/r_p. \quad [8]$$

Equation [8] shows the same linear dependence of $1/T_1$ with $1/r_p$ as given by Eq. [5] although the slope is different. For a cylindrical pore, a similar expression may be obtained by recognizing that the characteristic size, R, and the hydraulic radius, r_p, are equivalent:

$$1/T_1 = \alpha + \beta(1 - 2\Delta\alpha/\beta)/r_p + \Delta\beta(\Delta\alpha/\beta - \tfrac{1}{2})/r_p^2. \quad [9]$$

In practice, T_1 is known and r_p must be found using the quadratic equation and the constraint that the surface and bulk volume fractions must be between 0 and 1:

$$r_p = -\phi_2/(2\phi_1) + \sqrt{[\phi_2/(2\phi_1)]^2 - \phi_3/\phi_1}, \quad [10]$$

where

$$\phi_1 = \alpha - 1/T_1$$
$$\phi_2 = \beta(1 - 2\alpha\Delta/\beta)$$
$$\phi_3 = \Delta\beta(\Delta\alpha/\beta - \tfrac{1}{2}).$$

For a spherical cavity pore of radius R, the hydraulic radius, $2R/3$, and T_1 are related by

$$1/T_1 = \alpha + \beta(1 - 2\Delta\alpha/\beta)/r_p + \Delta\beta 4/3 \times [\Delta\alpha/\beta - \tfrac{1}{2}]/r_p^2 + \Delta^2\beta 8/27[\tfrac{1}{2} - \Delta\alpha/\beta]/r_p^3. \quad [11]$$

Equation [11] is a cubic equation with one real root which is given by

$$r_p = [-b + \sqrt{b^2 + a^3}]^{1/3} + [-b - \sqrt{b^2 + a^3}]^{1/3} - \phi_2/(3\phi_1), \quad [12]$$

where

$$a = (3\phi_3/\phi_1 - \phi_2^2/\phi_1^2)/9$$
$$b = (2\phi_2^3/\phi_1^3 - 9\phi_2\phi_3/\phi_1^2 + 27\phi_4/\phi_1)/54$$
$$\phi_1 = \alpha - 1/T_1$$
$$\phi_2 = \beta(1 - 2\Delta\alpha/\beta)$$
$$\phi_3 = \Delta\beta 4/3[\Delta\alpha/\beta - \tfrac{1}{2}]$$
$$\phi_4 = \Delta^2\beta 8/27[\tfrac{1}{2} - \Delta\alpha/\beta].$$

In addition to the slit, cylinder, and spherical cavity pore shapes considered above, another common pore model is the void space surrounding a packing of uniform solid spheres (8). The hydraulic radius of a pore in a sphere packing is related to the solid sphere radius, R_s, and the porosity of the sphere packing, ϵ, by

$$r_p = \tfrac{2}{3}\epsilon/(1 - \epsilon)R_s. \quad [13]$$

If the surface layer surrounding a sphere is assumed not to interact with the surface layer surrounding other spheres, the surface fraction, f_s, is given by

$$f_s = [3\Delta/R_s + 3(\Delta/R_s)^2 + (\Delta/R_s)^3](1 - \epsilon)/\epsilon. \quad [14]$$

Using Eqs. [1], [13], and [14],

$$1/T_1 = \alpha + \beta(1 - 2\Delta\alpha/\beta)/r_p + \tfrac{4}{3}\epsilon/(1 - \epsilon)\beta\Delta(\tfrac{1}{2} - \alpha\Delta/\beta)/r_p^2 + \tfrac{8}{27}[\epsilon/(1 - \epsilon)]^2\beta\Delta^2(\tfrac{1}{2} - \alpha\Delta/\beta)/r_p^3. \quad [15]$$

The radius may be determined using Eq. [12] with the constants

$$\phi_1 = \alpha - 1/T_1$$

$$\phi_2 = \beta(1 - 2\Delta\alpha/\beta)$$

$$\phi_3 = \tfrac{4}{3}\epsilon/(1 - \epsilon)\Delta\beta(\tfrac{1}{2} - \alpha\Delta/\beta)$$

$$\phi_4 = \tfrac{8}{27}[\epsilon/(1 - \epsilon)]^2\beta\Delta^2(\tfrac{1}{2} - \alpha\Delta/\beta). \quad [16]$$

For this sphere packing model, the relationship between pore size and the observed T_1 is a function of the porosity in addition to the relaxation parameters. However, since ϵ is usually either known or may be extracted from the spin-lattice relaxation measurements, ϵ is not an independent parameter.

EXPERIMENTAL—POROUS SOLID FABRICATION

For this project, a series of porous solids with a variety of pore size and size distribution in the mesopore/micropore size range was desirable. The sol–gel process for preparing inorganic glasses and ceramics employs monomeric metal alkoxides ($M(OR)_n$, where M is often Si, Al, B, etc., and R is often an alkyl group) as ceramic percursors and offers considerable control over structure development. In solution, the alkoxides are hydrolyzed and condensed to form inorganic networks composed of M–O–M bonds as shown by the reactions

$$M(OR)_n + xH_2O \rightarrow M(OR)_{n-x}OH_x + xROH \quad [17]$$

$$2M(OR)_{n-x}OH_x \rightarrow (RO)_{n-x}M\text{–O–}M(OR)_{n-x} + H_2O. \quad [18]$$

Depending on the synthesis conditions, (for example, H_2O/OR molar ratios, solution pH, temperature, etc.), the structure of the growing inorganic solution species may be varied from weakly branched chains to more highly branched clusters to fully condensed colloidal particles (9). When the growing units link together to form a network which spans the solution volume, the system gels forming a stiff jelly-like mass. Evaporation of solvent causes shrinkage of the gel primarily due to surface tension forces. Dried gels (xerogels) are typically highly porous solids characterized by extremely high surface areas (500–1000 m^2/g) (9).

The silica gels used in this study (identified as A2, A3, and B2) were prepared by hydrolysis and condensation of tetraethyl orthosilicate (TEOS) according to the procedures outlined elsewhere (10). The four-component (SiO_2, B_2O_3, Al_2O_3, BaO) xerogel (designated as C4) was prepared by a variation of the method described by Brinker and Mukherjee (10) in which sodium acetate was excluded from the reaction. After gelation, all samples were dried at 323 K and heated to 573 K at 1 K/min. Direct TEM microscopy of the xerogel samples showed a fine globular structure for A3, B2 (10), and C4 (11), whereas A2 (10) was observed to be featureless at all magnifications. These features reflect the structure of the polysilicate solution species prior to gelation: conditions employed for A3, B2, and C4 resulted in highly branched clusters; A2 conditions result in more weakly branched, compliant species which freely interpenetrate prior to gelation, completely obscuring their identity in the xerogel (12).

EXPERIMENTAL—PORE STRUCTURE CHARACTERIZATION

Spin-lattice relaxation measurements were made using an inversion-recovery experiment (180°-τ-90°). All measurements were made at a proton Larmor frequency of 20 MHz and a temperature of 303 K. A Spin-Lock Ltd. CPS-2 pulse NMR was used. The 90° and 180° radiofrequency measurement and inversion pulses were approximately 5 and 10 μs in duration. FIDs were collected using a Nicolet 2090 digital oscilloscope interfaced to an IBM CS-9000 computer. The delay time between pulse sequences was 10 s and the magnitude of τ was varied between 1 ms and 9 s. Forty to 50 different τ values were used to characterize the relaxation curve, $M(\tau)$. After an experiment, $M(\tau)$ is transferred to a VAX 8650 computer for determination of $f(T_1)$ using the regularization approach described by Gallegos and Smith (2). An error level in $M(\tau)$ of 0.01

was assumed for the calculation of the optimum regularization smoothing parameter.

In addition to NMR analysis, conventional pore structure analysis was undertaken using nitrogen adsorption/condensation, mercury porosimetry, and gas permeation. Nitrogen adsorption/condensation measurements were made at 77 K using both a Quantasorb flow-type analyzer and an Autosorb-6 volumetric adsorption apparatus. Before analysis, samples were outgassed at 383 K. Surface areas were calculated using the BET equation and a cross-sectional area of 0.162 nm^2 per molecule (13). Pore volume distributions for radius greater than 1 nm were calculated from both the adsorption and desorption branches of the isotherm using the BJH method and micropore size distribution was attempted using $V - t$ plots (13). Mercury porosimetry experiments were conducted over the pressure range of 12 to 33,000 psia (9 $\mu m > r > 3.3$ nm) using a Quantachrome Autoscan-33 scanning porosimeter. Before intrusion, the sample were evacuated at 383 K and 10 μm mercury for 1 h. For pore size calculations, the mercury contact angle was taken to be 140°.

RESULTS

The reason for developing the pore shape models given above is to relate the effects of pore shape on the relative fractions of fluid in the bulk and surface phases (f_b and f_s). In our development, f_b is given by $(1 - \Delta/R)^n$ for the simple pore geometries where n depends on the geometry. Almagor and Belfort (7) have studied relaxation of adsorbed water using a series of Vycor-type glasses with different pore sizes. Instead of the more simplistic and straightforward two-phase model employed in this work, Almagor and Belfort employed a three-phase model. By varying the relative humidity of water vapor in contact with their samples, the quantity of water in the samples was varied from a monolayer to complete saturation. By measuring T_1 as a function of moisture content, f_b was determined for six samples with mean hydraulic radius in the range of 1.2 to 12.6 nm. f_b was found to increase from 0.2 to 0.96 with increasing pore size. For each pore geometry (i.e., slab, cylinder, spherical cavity), we have fit the expression $(1 - \Delta/R)^n$ to Almagor and Belfort's measurements by treating the thickness of the surface-affected phase, Δ, as a variable which is selected such that the deviation between experiment and theory is minimized by a least-squares criterion. The results of this comparison are presented in Fig. 1. The best fit surface thickness values were 0.476 nm for a slab pore model, 0.590 nm for the cylinder, and 0.624 nm for the spherical cavity. Agreement between experiment and the various pore models is certainly within the experimental accuracy of these kinds of measurements and demonstrates the validity of this type of model for predicting pore shape effects on the distribution between the surface and bulk phases.

To assess the accuracy of the approximate $T_1 - r_p$ relationship given by Eq. [5] for use in the mesopore/micropore size range, we have plotted T_{1b}/T_1 versus $1/r_p$ for various pore geometries and typical relaxation parameters in Fig. 2. When plotted in this manner, Eq. [5] will have a slope of β/α and an intercept of one. Relaxation parameters used are Δ equal to 0.3 nm, β equal to 12.63 nm/s, and α equal to 0.485 s^{-1}, which correspond to values reported for a series of controlled pore glass samples which are not microporous (1). For pore size greater than 5 nm, the volume of the surface-phase fraction is small and the variation of T_1 with pore size is essentially independent of pore geometry. As expected, the deviation between the slab or flat plate pore model and the approximate (linear) expression is minor over the entire pore size range studied. For the cylindrical and spherical pore models, deviations between the approximate and exact expressions only become significant in the microporous size range. For a given T_1 value, the approximate expression will overpredict the pore size. For the solid sphere packing pore model, the degree of deviation between the linear approximation and the exact expression is a function of porosity. We present results for a range of porosity corresponding to the

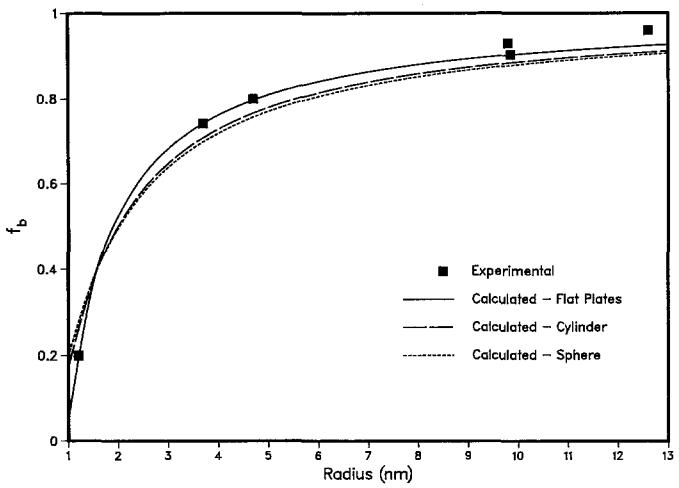

FIG. 1. Volume fraction in bulk phase for various model geometries and experimentally determined (Almagor and Belfort (7)).

practical limits for a random packing of spheres. The truncation points for these curves correspond to a surface-phase volume fraction equal to one. Only for relatively high porosity are deviations between the exact and approximate expressions significant in the mesopore size region. For lower porosity, the deviations between the approximate and exact solution are on the same order as for the cylindrical pore model. However, for the solid sphere packing pore model, the approximate solution will underpredict the pore size for a given T_1 value. Although different α and β values will vary these results slightly, the same qualitative finding is observed. The effect of changing Δ is most pronounced in the micropore region. The ultimate accuracy of the NMR spin-lattice relaxation approach to microporous materials will be fixed by the degree of certainty concerning Δ and pore shape.

Nitrogen sorption/condensation measurements were made for each sample used in this

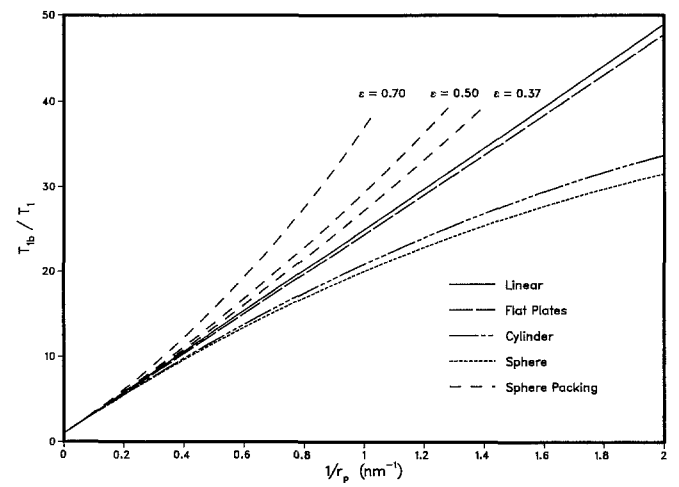

FIG. 2. Observed spin-lattice relaxation time, T_1, as related to mean pore radius for various model geometries.

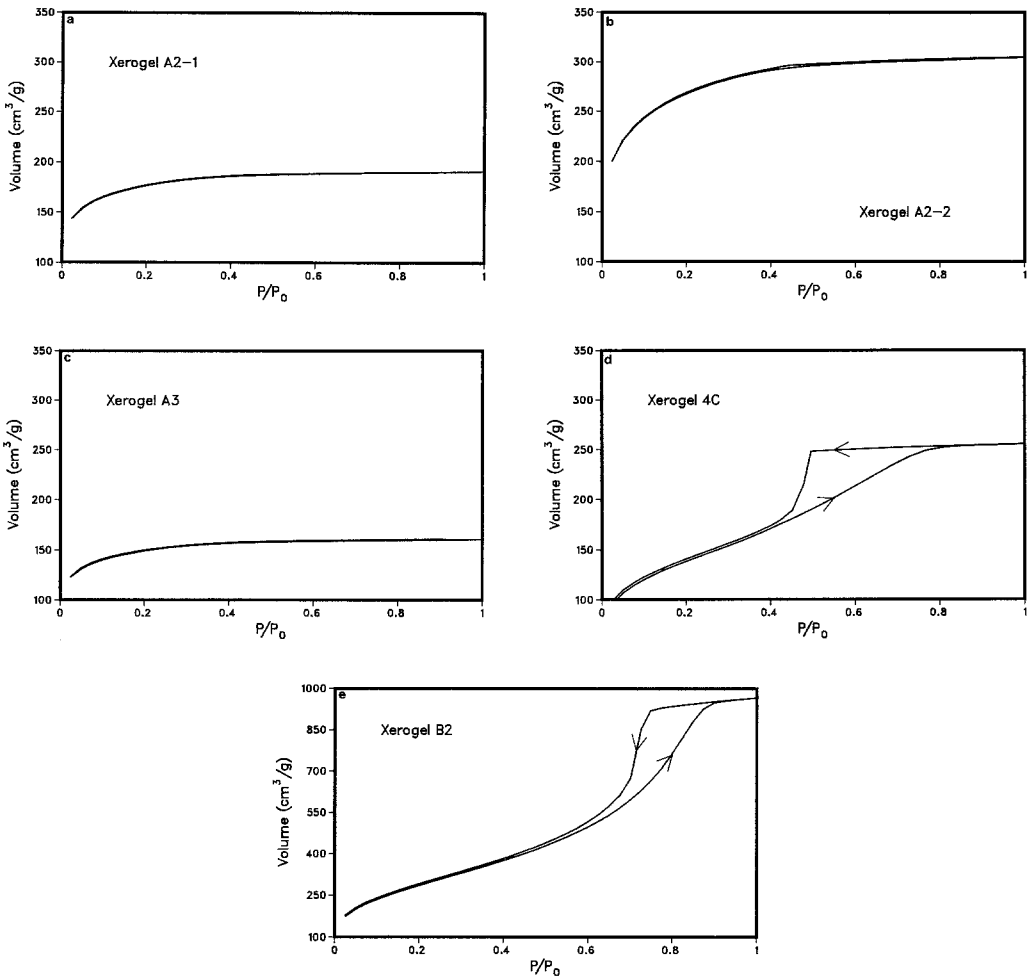

FIG. 3. (a) N_2 sorption isotherm for sample A2-1. (b) N_2 sorption isotherm for sample A2-2. (c) N_2 sorption isotherm for sample A3. (d) N_2 sorption isotherm for sample 4C. (e) N_2 sorption isotherm for sample B2.

study. Sorption isotherms for the various samples are presented in Figs. 3a–e. The A2-1, A2-2, and A3 silica xerogel samples exhibit a high degree of microporosity and little hysteresis. In contrast, the four-component xerogel, 4C, has a broad hysteresis loop indicating pores in the 1- to 5-nm size range. The base-catalyzed silica xerogel, B2, also has a broad hysteresis loop with a wide pore size range between 1 and 10 nm. The adsorption branch of the isotherms has been analyzed using the BET theory. Calculated surface areas as well as the total pore volume ($r < \approx 200$ nm), hydraulic radius ($r_p = 2PV/SA$), and the optimum value of the regularization parameter, δ_{opt} (2), used to generate NMR pore size distributions are presented in Table I. Although the two A2 samples, which were aged under different conditions, appear to be quite similar based upon the mean pore radius, mercury porosimetry measurements did not support this. As we intended, a series of samples with similar surface chemistry but widely varying pore structure has been obtained.

In order to relate the $f(T_1)$ distribution to the desired pore size, the parameters of α, β, and Δ must be determined. In past studies, this was accomplished using porous solids with

TABLE I

Sample Properties from Nitrogen Adsorption and Regularization Parameter, δ_{opt}

Sample	*SA*-BET (m^2/g)	*PV* (cm^3/g)	r_p (nm)	δ_{opt}
A2-1	654.9	0.296	0.90	0.0003
A2-2	989.2	0.472	0.95	0.0003
A3	552.9	0.248	0.90	0.00006
4C	501.7	0.395	1.57	0.030
B2	1020.8	1.495	2.93	0.006

a narrow pore size distribution and known surface area/total pore volume (1) and solid powders of known surface area (14). By independently measuring T_{1b}, α is obtained. Using Eq. [5] with α, the measured T_1, and the mean pore radius, β, is obtained. However, for porous solids with mesopores and/or micropores and if β is not known, a pore shape assumption and Δ value must be assumed before β may be back-calculated from the observed T_1. For this work, α was found to be 0.485 s. The A2-1 and A3 samples had very narrow pore size distributions, similar mean pore size, and similar average T_1. Therefore, we calculate β from the average of these results for different pore geometries and surface thickness. In principle, β values calculated from the A2-1 and A3 samples should be equal. Individual β values were within 5% of the mean value. The results of these calculations are presented in Table II. The β values found for these sol–gel materials are 2 to 3 times smaller than the values found for the controlled pore glass samples reported previously for the same temperature and proton frequency (1). This is presumedly the result of trapped solvent in these materials.

Figure 4 represents NMR-generated pore size distributions for the A2-1 silica xerogel sample using a surface thickness of 0.3 nm and the various pore geometries given in Table II. The porosity of this sample is $\approx$0.39 and we use 0.4 for the solid sphere packing model. Since we calculate β from the average of β for this sample and A3, the fact that the PSD maximum agrees so well with mean pore radius (i.e., $r \approx 0.9$ nm) should be expected. However, the lack of a significant variation of the PSD shape with pore geometry is not anticipated. If the pore size of the sample is closer to the value of Δ, pore geometry effects will be greater. We should note that the hydraulic radius is used in Fig. 4, and if the various pore model characteristic lengths are used, the curves would be quite different.

The β value back-calculated from relaxation measurements with a given material of known surface area and pore shape assumption is also a function of the surface-affected phase thickness, Δ. Figure 5 represents calculated NMR pore size distributions for the A2-1 sample when a cylindrical pore shape assumption is made and Δ is varied. As before, the pore radius associated with the PSD maximum is independent of changing relaxation parameters since we are back-calculating from the measured mean T_1's for A2-1 and A3. Also, the shape of the distribution is relatively insensitive to Δ.

The results of Figs. 4 and 5 imply that when one is back-calculating spin-lattice relaxation parameters from well-defined porous solids, the assumption of Δ is not critical except when the pore size approaches Δ in magnitude. However, the pore shape assumption does appear to be important if the "correct" value of β is to be determined which can then be applied to other porous solids with similar surface chemistry but different pore size and shape. This is illustrated in Fig. 6. NMR-de-

TABLE II

Average β Values Calculated from A2-1 and A3 Using Various Pore Geometries and Δ Values

Pore model	Δ (nm)	β (nm/s)
Linear	0.3	3.22
Flat plates	0.3	3.52
Cylinder	0.3	4.16
Spherical	0.3	4.35
Sphere pack. (ϵ = 0.4)	0.3	3.08
Cylinder	0.1	3.51
Cylinder	0.2	3.82

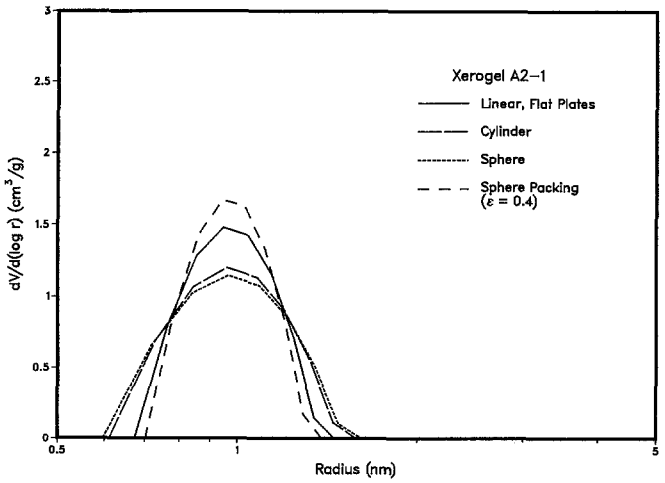

FIG. 4. NMR-generated pore size distributions for A2-1 with constant Δ (=0.3 nm) and β adjusted for geometry.

rived pore size distributions are calculated from the A2-1 relaxation data using various pore shapes and a β value of 4.16 (i.e., obtained from the cylindrical pore assumption and Δ equal to 0.3). As expected, significant differences are observed between the PSDs calculated using the different pore geometries. However, this result is essentially the same result as observed when interpreting nitrogen condensation data with different pore shape models and is a consequence of using the hydraulic radius to characterize the pore size. Alternatively, when one assumes a pore shape, the actual characteristic length for that model could be employed.

Pore size distributions (PSD) for the A2-1 silica xerogel, as obtained from both spin-lattice relaxation measurements and nitrogen sorption analysis, are presented in Fig. 7. Mercury porosimetry for this sample indicated negligible intrusion for pressures up to 33,000 psia ($r \approx 3$ nm) and is not included on the

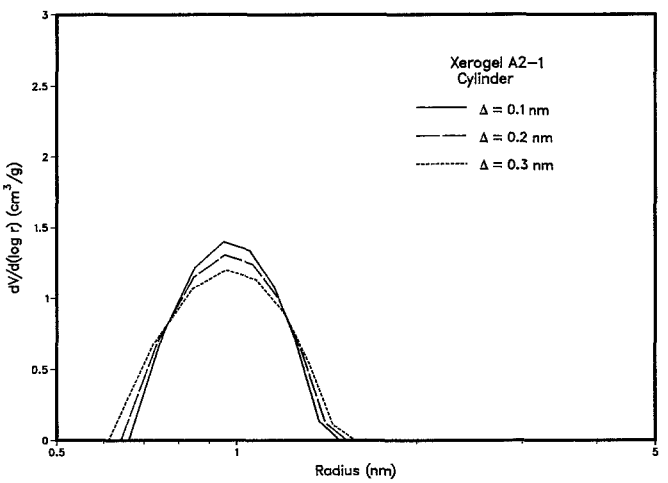

FIG. 5. NMR-generated pore size distributions for A2-1 with fixed geometry (cylinder) and β adjusted for Δ.

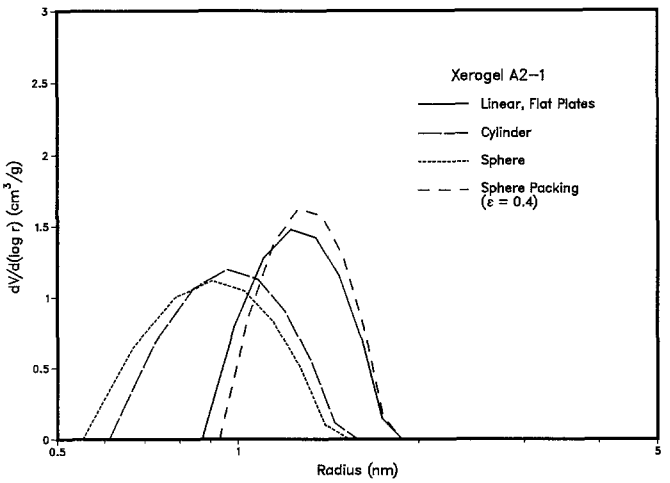

FIG. 6. NMR-generated pore size distributions for A2-1 with constant β (=4.16) and constant Δ (=0.3 nm).

plot. Pore size analysis using the Kelvin equation and the N_2 adsorption and desorption isotherms are virtually identical as expected from the lack of hysteresis in the isotherms. The NMR PSD is calculated assuming a cylindrical pore model, a β value of 4.16 nm/s, Δ of 0.3 nm, and α of 0.485 s^{-1}. In contrast to the results of the micropore analysis (t-plot), the NMR analysis indicates no porosity in pores with hydraulic radius less than 0.5 nm. Agreement of the NMR results with the sorption generated PSD is on the same order as the agreement between the t-plot and BJH analysis.

Figure 8 is a similar series of PSDs generated via various techniques for the second A2 sample, A2-2. Unlike A2-1, mercury porosimetry indicates significant porosity in the mesopore range although intrusion is still occurring at the lower 3-nm pore size cutoff. For this sample, the mercury porosimetry and N_2 adsorption/desorption PSDs are approximately an

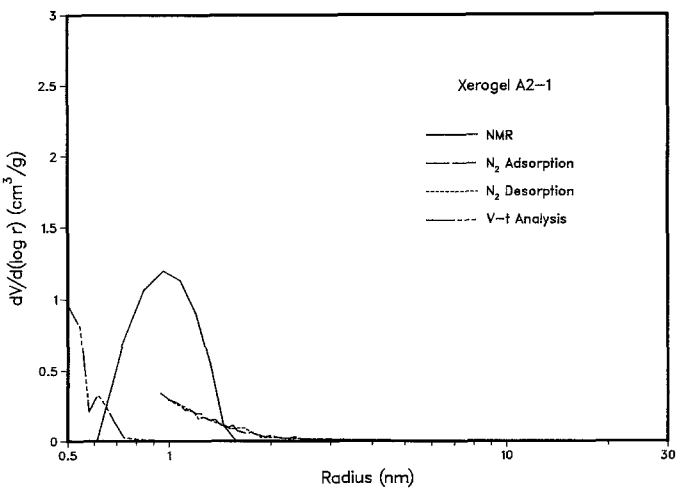

FIG. 7. Pore size distributions for sample A2-1.

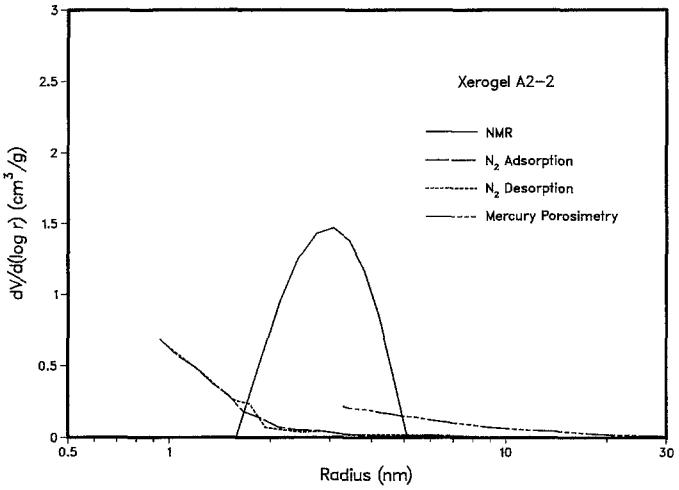

FIG. 8. Pore size distributions for sample A2-2.

order of magnitude different. The NMR PSD, which was calculated using the cylindrical pore assumption and the same parameters as the A2-1 sample, is between the nitrogen and mercury results. For this sample, NMR results indicate a small fraction of pores (≈2.3%) with radius less than 0.5 nm.

As with the A2-1 sample, no mercury intrusion is noted for the A3 silica xerogel and porosimetry results are not included. Figure 9 contains NMR- and sorption-generated pore size distributions. The results are virtually identical with those for the A2-1 sample except for a slightly narrower PSD observed with all methods.

The base-catalyzed silica xerogel, B2, and the four-component xerogel, 4C, exhibit quite different pore structure than the A2 and A3 materials. The most interesting results of this work are found with the B2 sample (see Fig. 10). This material has a very high specific surface area (>1000 m^2/g) yet a fairly large pore size (see Table I). Mercury porosimetry indicates a fairly flat PSD in the size range of 3 to

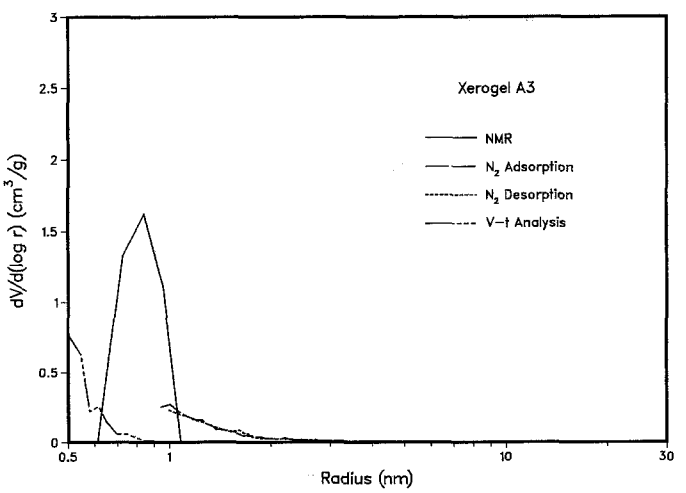

FIG. 9. Pore size distributions for sample A3.

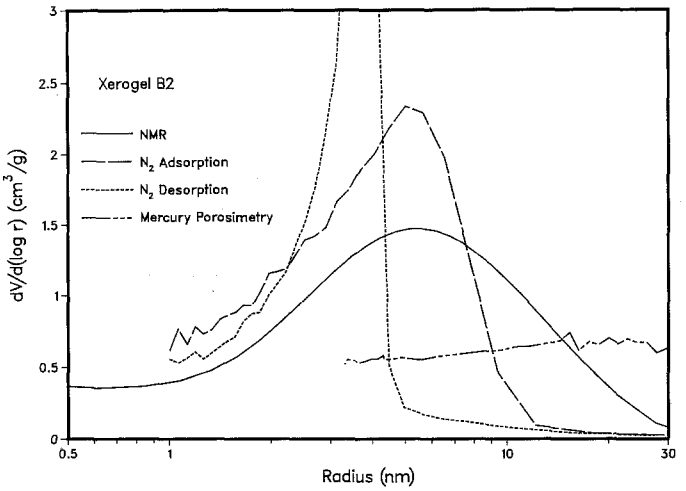

FIG. 10. Pore size distributions for sample B2.

$\approx$100 nm. In contrast, analysis of the desorption isotherm indicates a narrow PSD in the pore radius range of 1 to 5 nm. A smaller tail is noted up to 30 nm. The adsorption branch indicates a slightly wider distribution over the radius range of 1 to $\approx$13 nm with a similar tail to 30 nm. Micropore analysis, *t*-plot, of this isotherm was not successful (i.e., indicated a negative micropore volume). The NMR-derived PSD (using the same pore shape assumption and parameters as the other samples) showed very good agreement with the PSD calculated from the adsorption branch of the isotherm. In addition, NMR analysis indicates the presence of pores in both the 0.5- to 1.0-nm and less than 0.5-nm pore size ranges. Approximately 5.7% of the pore volume is found in pores less than 0.5 nm. This NMR result certainly agrees with the very high surface areas obtained with this sample.

Figure 11 contains pore size distributions for the 4C sample. Unfortunately, mercury porosimetry could not be conducted on this particular 4C sample but mercury analysis on similar 4C samples indicates a significant fraction of porosity in the 10- to 30-nm size range.

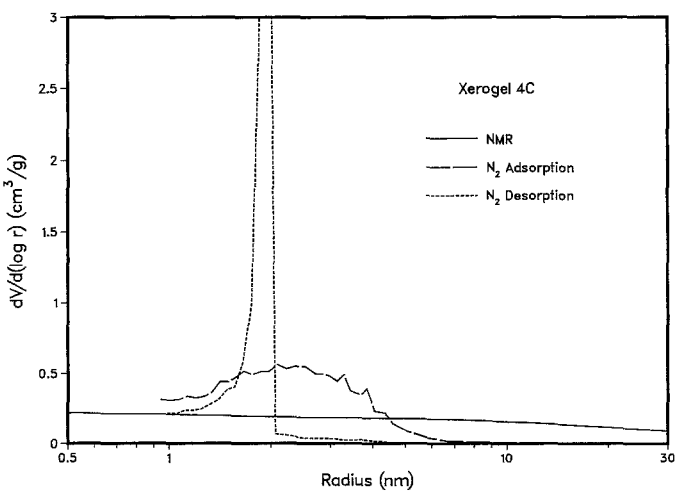

FIG. 11. Pore size distributions for sample 4C.

However, analysis of the nitrogen desorption isotherm indicates a very narrow distribution between 1.6 and 2.0 nm. The adsorption branch indicates a broader distribution between 1 and 7 nm. The NMR PSD is very broad as reflected in the large δ_{opt} value (0.03). Approximately 25% of the pore volume is in pores less than 0.5 nm. The pores at radius greater than 10 nm predicted with NMR technique, while not matching the sorption results, are on the same order as porosimetry results for similar 4C samples. The agreement between NMR-derived PSDs and nitrogen sorption and mercury porosimetry for the A2-2, B2, and 4C samples is particularly encouraging when one considers that all spin-lattice relaxation parameters were obtained only from the average of the A2-1 and A3 results.

SUMMARY

By comparing previously published results of the relative distribution of surface- and bulk-phase water as a function of pore size (7) to predictions from various pore models, we have demonstrated that the "two-fraction, fast exchange" model may be applied to relate measured T_1 to pore size in the mesopore and micropore size range if the pore geometry is known (or assumed). The comparison between conventional techniques, such as nitrogen sorption and mercury porosimetry, and the results of NMR spin-lattice relaxation experiments is complicated by the fact that different pore structure parameters are measured with these methods. Despite this, agreement between the methods is quite good for the 5 sol–gel-derived materials which we have studied.

APPENDIX: NOMENCLATURE

f_b = Volume fraction of pore fluid with bulk properties
f_s = Volume fraction of pore fluid with surface-affected properties
$f(T_1)$ = Volume distribution of T_1
PV = Specific pore volume
r_p = Hydraulic radius, $2PV/SA$
R = Characteristic pore model size
R_s = Solid sphere radius
SA = Specific surface area
T_1 = Observed spin-lattice relaxation decay time
T_{1b} = Spin-lattice relaxation time for bulk fluid
$T_{1s} = T_{1\ surface}/\Delta$
$T_{1\ surface}$ = Surface-affected spin-lattice relaxation time
$\alpha = 1/T_{1b}$
$\beta = 2/T_{1s}$
Δ = Thickness of surface phase
δ_{opt} = Optimum value of the regularization smoothing parameter
ϵ = Porosity

ACKNOWLEDGMENTS

This work has been funded by the Sandia National Laboratories under Grant 04-9245. The authors thank J. Shields of Quantachrome Inc. for providing some nitrogen adsorption measurements, T. Holt of UNM for performing the mercury porosimetry measurements, and P. Davis of UNM for conducting some of the NMR experiments.

REFERENCES

1. Gallegos, D. P., Munn, K., Smith, D. M., and Stermer, D. L., *J. Colloid Interface Sci.* **119,** 127 (1987).
2. Gallegos, D. P., and Smith, D. M., *J. Colloid Interface Sci.* **122,** 143, (1988).
3. Munn, K., and Smith, D. M., *J. Colloid Interface Sci.* **119,** 117 (1987).
4. Brown, J. A., Brown, L. F., Jackson, J. A., Milewski, J. V., and Travis, B. J., *in* "Proceedings, the SPE/DOE Unconventional Gas Recovery Symposium, 1982," p. 201.
5. Brownstein, K. R., and Tarr, C. E., *J. Magn. Reson.* **26,** 17 (1977).
6. Woessner, D. E., *J. Magn. Reson.* **39,** 297 (1980).
7. Almagor, E., and Belfort, G., *J. Colloid Interface Sci.* **66,** 146 (1978).
8. Haynes, J. M., *Spec. Period Rep.: Colloid Sci.* **2,** 101–129 (1975).
9. Brinker, C. J., and Scherer, G. W., *J. Non-Cryst. Solids* **70,** 301 (1985).
10. Brinker, C. J., Keefer, K. D., Schaefer, D. W., and Ashley, C. S., *J. Non-Cryst. Solids* **48,** 47 (1982).
11. Brinker, C. J., and Mukherjee, S. P., *J. Mater. Sci.* **16,** 1980 (1981).
12. Brinker, C. J., Keefer, K. D., Schaefer, D. W., Assink, R. A., Kay, B. D., Ashley, C. S., *J. Non-Cryst. Solids* **63,** 45 (1984).
13. Lowell, S., and Shields, J. E., "Powder Surface Area and Porosity." Chapman & Hall, London, 1984.
14. Davis, P. J., Gallegos, D. P., and Smith, D. M., *Powder Technology,* **53,** 39, (1987).